Modification of a commercial atomic force microscopy for low-noise, high-resolution frequency-modulation imaging in liquid environment

S. Rode,[1] R. Stark,[2] J. Lübbe,[3] L. Tröger,[3] J. Schütte,[4,a)] K. Umeda,[4] K. Kobayashi,[4] H. Yamada,[4] and A. Kühnle[4,b)]
[1]*Institut für Physikalische Chemie, Fachbereich Chemie, Johannes Gutenberg-Universität Mainz, Jakob-Welder-Weg 11, 55099 Mainz, Germany*
[2]*GKC/O - G201, BASF SE, 67056 Ludwigshafen, Germany*
[3]*Fachbereich Physik, Universität Osnabrück, Barbarastraße 7, 49076 Osnabrück, Germany*
[4]*Department of Electronic Science and Engineering, Kyoto University, Katsura, Nishikyo, Kyoto 615-8510, Japan*

(Received 27 April 2011; accepted 22 May 2011; published online 12 July 2011)

A key issue for high-resolution frequency-modulation atomic force microscopy imaging in liquids is minimizing the frequency noise, which requires a detailed analysis of the corresponding noise contributions. In this paper, we present a detailed description for modifying a commercial atomic force microscope (Bruker MultiMode V with Nanoscope V controller), aiming at atomic-resolution frequency-modulation imaging in ambient and in liquid environment. Care was taken to maintain the AFMs original stability and ease of operation. The new system builds upon an optimized light source, a new photodiode and an entirely new amplifier. Moreover, we introduce a home-built liquid cell and sample holder as well as a temperature-stabilized isolation chamber dedicated to low-noise imaging in liquids. The success of these modifications is measured by the reduction in the deflection sensor noise density from initially 100 fm/$\sqrt{\text{Hz}}$ to around 10 fm/$\sqrt{\text{Hz}}$ after modification. The performance of our instrument is demonstrated by atomically resolved images of calcite taken under liquid conditions.
 [doi:10.1063/1.3606399]

I. INTRODUCTION

Recent progress in constructing optical beam deflection (OBD) sensors used in atomic force microscopes (AFM)[1–5] has opened up new possibilities in studying the solid-liquid interface on the atomic scale.[6–8] It has been shown that optimized readout electronics constitute a key feature to achieve true atomic resolution in liquid environment.[9] Besides atomic-resolution imaging, the new generation of instruments provide other very promising tools, such as 3D force mapping in liquids.[10] Optimized AFMs have even proven sensitive enough for resolving very weakly adsorbed water layers (hydration layers) on surfaces.[10,11]

The figure of merit in optimizing the AFM electronics is the deflection sensor noise density, which is the electronic noise arising from the readout electronics. Most commercially available AFMs exhibit deflection sensor noise densities in the range of 100–1000 fm/$\sqrt{\text{Hz}}$, making these instruments inappropriate for high-resolution frequency-modulation imaging in liquids. The three main noise sources in a deflection sensor system are (1) the light source, (2) the photodiode and amplifiers and for coherent light sources (3) interference.

However, high-resolution frequency-modulation (FM) imaging in liquids not only requires low-noise electronic components. All other parts of the AFM have to be adjusted with the high-resolution application in mind. Obviously, the scanner (primary the digital-to-analog converter) itself has to have atomic-resolution imaging capability. The entire AFM needs to be vibration isolated and temperature stabilized in order to reduce mechanical noise and thermal drift. Finally, an important issue is the excitation of the cantilever oscillation, as FM imaging relies on detecting very small frequency shifts. In this respect, the design of the cantilever holder is of importance.

In this paper, we present all modifications necessary for improving a commercially available AFM for atomic-resolution FM AFM imaging in liquids. The deflection sensor noise density was reduced from initially 100 fm/$\sqrt{\text{Hz}}$ to around 10 fm/$\sqrt{\text{Hz}}$, illustrating the success of the electronic noise reduction. We demonstrate the performance of the entire system including liquid cell, cantilever holder and isolation box by presenting atomically resolved images of calcite taken in liquids.

The paper is organized as follows. In Sec. II, we give a brief theoretical introduction of the noise components contributing to the frequency noise. In Sec. III, the experimental setup is described that was modified in order to allow for FM AFM imaging with true atomic resolution. Then in Sec. IV, the modifications are presented in details. This includes all electronic parts responsible for the signal detection in the scanhead as well as construction details of the liquid cell with cantilever holder, sample holder and isolation box. Finally, we demonstrate the performance of the modified system by presenting true atomic-resolution imaging on calcite under liquid conditions in Sec. V.

II. THEORETICAL BACKGROUND

In FM AFM imaging, the image quality is mainly influenced by the frequency noise (δf) at the output of the signal

a)Present address: Dr. Eberl MBE-Komponenten GmbH, Gutenbergstraße 8, 71263 Weil der Stadt, Germany.
b)Electronic mail: kuehnle@uni-mainz.de.

demodulator. In a frequency-modulated signal, the instantaneous frequency is a sum of a time-independent carrier frequency (f_0) and a modulation with a modulation frequency f_m and a modulation amplitude Δf. For modulation frequencies f_m smaller than the corner frequency $f_c = f_0/(2Q)$, the frequency noise can be calculated by[12]

$$D^f_{tot} = \frac{k_B T f_0}{\pi k Q A_0^2} + \frac{f_0^2}{2Q^2 A_0^2} D^z_{el} + \frac{2 f_m^2}{A_0^2} D^z_{el}, \qquad (1)$$

where D^f_{tot} is the total power spectral density of the frequency noise at the demodulator output, k, Q and f_0 are the spring constant, the quality factor and the resonance frequency of the cantilever, A_0 and D^z_{el} are the oscillation amplitude and power spectral density of the deflection sensor noise, respectively.

As discussed by Kobayashi *et al.*[12] for describing the frequency noise, it is important to distinguish two regimes, characterized by having the displacement noise inside or outside of $[f_0 - f_c, f_0 + f_c]$. The corner frequency f_c describes the bandpass characteristics of the cantilever. Exciting the cantilever at frequencies outside of $[f_0 - f_c, f_0 + f_c]$ results in a damped oscillation amplitude, while excitation of the cantilever with frequencies inside of $[f_0 - f_c, f_0 + f_c]$ cause a maximum or only slightly damped oscillation amplitude. The corner frequency marks the point, at which the signal is damped by –3dB compared to the maximum oscillation amplitude. In the following, the letter D indicates a power spectral density, whereas d indicates an amplitude spectral density, i.e., the power spectral density of the deflection sensor noise D^z_{el} is the square of the deflection sensor noise density d^z_{el}, $D^z_{el} = (d^z_{el})^2$.

Integrating the power spectral density of the frequency noise (1) over the measurement bandwidth reveals the averaged frequency noise

$$\delta f = \sqrt{\frac{k_B T f_0 B}{\pi k Q A_0^2} + \frac{f_0^2 B}{2Q^2 A_0^2} D^z_{el} + \frac{2B^3}{3A_0^2} D^z_{el}}, \qquad (2)$$

where B is the measurement bandwidth.

The first term under the root in the above equation describes the thermal noise contribution (δf_{th}). The second term constitutes the contribution of phase fluctuations to the frequency noise (δf_{SOL}), which originates from using a self-oscillation loop to excite the cantilever. The third term arises from the influence of the deflection sensor noise to the frequency noise (δf_{el}). It should be noted that the second term only applies for $f_m < f_c$, which is typically valid in liquid environment because of the large damping.[12] To calculate the frequency noise in a high Q environment, only the first and third terms need to be considered.

Figure 1 shows the calculated frequency noise in dependence on the deflection sensor noise density for typical cantilevers in low Q (blue) and high Q (red) environment. The total frequency noise in low Q environments is always larger than the corresponding noise in high Q environments due to the large thermal noise contribution in a low Q environment as given by the first term in Eq. (2).

For large deflection sensor noise densities the slope of the blue curve is much larger than the slope of the red curve, indicating that optimizing the deflection sensor noise density is most effective in low Q environment. Due to the large damping of the cantilever in a low Q environment phase fluctuations cause large frequency noise. This behavior is expressed in the second term of Eq. (2), which dominates the frequency noise for large deflection sensor noise densities in a low Q environment as shown in Fig. 1.

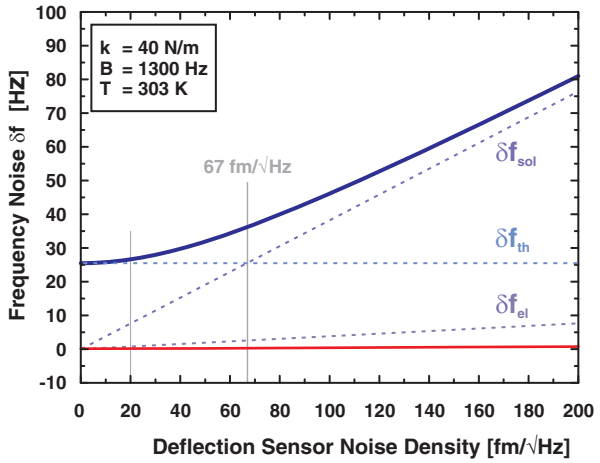

FIG. 1. (Color online) Frequency noise for a low Q cantilever (upper curve, $Q = 10$, $f_0 = 150$ kHz, $A_0 = 1$ nm) and a high Q cantilever (lower curve, $Q = 10000$, $f_0 = 300$ kHz, $A_0 = 10$ nm) as a function of deflection sensor noise density (as amplitude noise density). Both, frequency noise for low Q and high Q environment, was calculated for typical experimental conditions.

The third term, describing the frequency noise contribution of the deflection sensor noise, can be neglected in low Q environments, but it is dominating the frequency noise in high Q environments for large deflection noise densities.

As the above discussion implies, the frequency noise needs to be reduced for high-resolution imaging. However, several approaches to reduce the frequency noise (e.g., increasing the oscillation amplitude, decreasing the measurement bandwidth) decrease at the same time the relevant signal. Thus, instead of considering the frequency noise solely, the signal-to-noise ratio (SNR) needs to be optimized for high-resolution images.

Decreasing the temperature to reduce the thermal noise is obviously limited by the freezing point of the liquid used. Another way to reduce the thermal noise is to increase the spring constant k of the cantilever. The latter approach, however, also reduces the frequency shift signal,[13] as the signal is proportional to $1/k$ whereas the noise is proportional to $1/\sqrt{k}$ (see Eq. (2)), indicating that the SNR becomes higher for smaller k.

Besides this, the signal can be increased by decreasing the amplitude, again improving the SNR.[13] However, decreasing both the spring constant and the amplitude simultaneously is difficult, because the attractive forces between tip and sample pull the tip towards the sample. In order to avoid snap-into-contact, the restoring force of the cantilever (kA_0) has to be larger than the tip-sample force. Typical experimental values that have revealed atomic-resolution imaging in liquids are spring constants around 40 N/m and oscillation amplitudes in the order of $A_0 < 1$ nm.

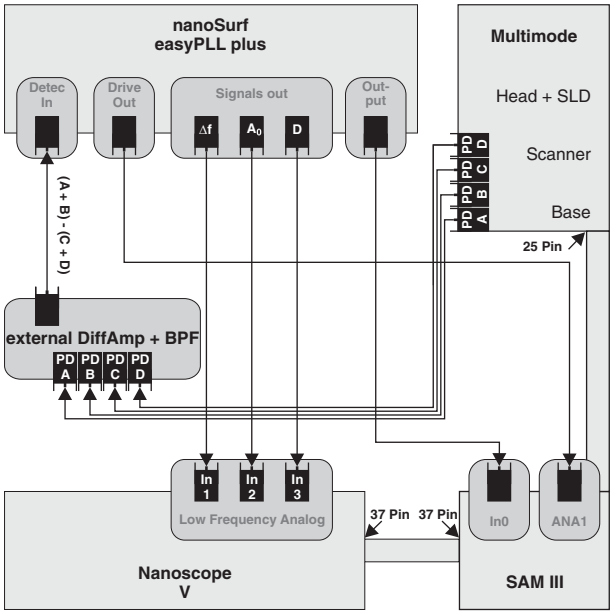

FIG. 2. Wiring diagram of the used setup. The developed scanhead is connected to an external differential amplifier and additional bandpass filter. The filtered signal is fed into the easyPLL plus. The output signal of the easyPLL plus is connected to the In0 input of the Nanoscope V controller at the signal access module (SAM) III. The drive out signal of the easyPLL plus is fed into ANA1 at SAM III, thus exciting the cantilever. Additional signals [frequency shift (Δf), amplitude (A_0) and dissipation (D)] can be recorded by using the low-frequency analog inputs of the Nanoscope V controller.

To conclude, improving the AFM readout electronics results in a smaller deflection sensor noise density, hence the frequency noise is effectively reduced and the SNR is increased correspondingly. Improving the deflection sensor noise is most effective in low Q environment as can be seen in Fig. 1. Above 67 fm/$\sqrt{\text{Hz}}$, the frequency noise in low Q environment is determined by the frequency noise of the self-oscillation loop (δf_{SOL}). At smaller deflection sensor noise densities, the thermal noise contribution is dominant. Optimizing the instrument below 20 fm/$\sqrt{\text{Hz}}$ only has a minor effect to the frequency noise, since the frequency noise is then saturated by the thermal noise, which cannot be affected by improving the electronics.

III. EXPERIMENTAL SETUP

In the present work, a commercial AFM MultiMode V from Bruker (Bruker Nano Surfaces Division, USA) with a Nanoscope V controller was modified. For signal demodulation, the AC signal from the differential amplifier is fed into a phase-locked loop (PLL) easyPLL electronics from Nanosurf (Nanosurf AG, Switzerland), compare Fig. 2. The oscillation amplitude is kept constant by driving the cantilever oscillation in the constant-amplitude mode using the easyPLL amplitude controller. The amplitude (A_{set}) and frequency shift (Δf_{set}) setpoints can be set manually at the easyPLL. The output signal from the easyPLL – measured frequency shift minus frequency shift setpoint - is connected to the input (In0) of the Nanoscope V controller. The Nanoscope software runs in contact mode, and the z-feedback setpoint is set to 0 V, resulting in constant frequency shift images.

IV. MODIFICATIONS

For improving the deflection sensor noise density of the AFM under consideration, all parts involved in the signal generation have to be analyzed and optimized in terms of their noise contribution. We start with explaining the changes made to the scanhead, including the light source, the photodiode and the amplifier electronics. Besides the improvement of the AFM's electronics, also some mechanical parts are crucial for high-resolution imaging in liquid environment. This includes the design of the liquid cell as it serves as cantilever holder, the sample holder and the overall isolation of the AFM system from the environment. All these parts will be addressed in the following.

A. Scanhead and amplifier electronics

The original Bruker scanhead of the used MultiMode V system has a deflection sensor noise density of approximately 100 fm/$\sqrt{\text{Hz}}$. It is equipped with a radio frequency (RF) modulated laser diode and has a very large photodiode suitable for many different AFM modes such as contact, tapping, torsional modes, and others. Although the noise performance is not optimal, the mechanics of the original scanhead are very well developed and guarantee stability and ease of operation. It is, thus, reasonable to adopt these mechanical parts or only slightly modify them. For this reason, the home-built scanhead is very similar to the original Bruker design as can be seen in Fig. 3.

The light source was changed to allow for external temperature stabilization and integration of a Faraday isolator. Moreover, we decided to use a super luminescent diode (SLD) to reduce the coherence length of the light, thus, reducing *optical interference noise*. As light source, a commercial SLD (SLD-260-HP1-TOW2-PD) from S&K (Schäfter&Kirchhoff, Germany) is used. The SLD has a center wavelength of 684.1 nm, a spectral bandwidth of 8.1 nm and a very small coherence length, which is presumably an order of magnitude smaller than the coherence length of the radio frequency-modulated laser used in the original setup. A Faraday isolator (48FI-5-670, S&K, Germany) attenuates back reflected light from the cantilever to the SLD, lowering the *optical feedback noise*. Temperature stabilization is maintained by a Peltier element, which is integrated in the SLD cage.

The light beam from the SLD is fed into a special optic (fiber collimator: 60 FC-4-M12-10, micro-focus optic: 5M-M60-13-S, S&K, Germany) by a polarization-maintaining single mode fiber cable (PMC-630, S&K, Germany) and irradiates a prism, mounted on the scanhead (Bruker original), as shown in the lower part of Fig. 3. The prism deflects the beam onto the cantilever. From there, the reflected beam is directed by a mirror (Bruker original) to the photodiode (S4349, Hamamatsu, Japan). The spot size on the backside of the cantilever is $\approx 20\ \mu$m. The beam diameter, measured directly in front of the photodiode, is around one mm. It should be

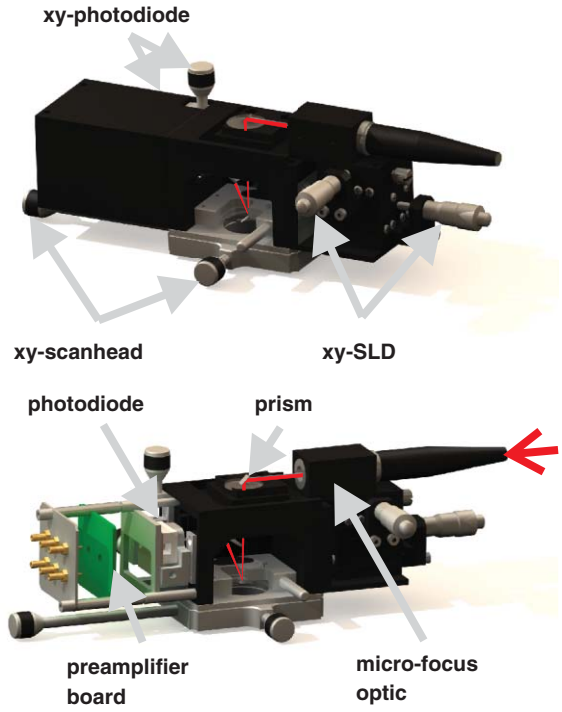

FIG. 3. (Color online) Model of home-built scanhead. In the upper part, the knobs for adjusting the photodiode, the SLD beam and the entire scanhead are indicated. In the lower part, the positions of the micro-focus optic, the prism, the photodiode and the preamplifier board are shown.

noted that the reflected beam shape is not perfectly round but elliptical, although the used optics produce a Gaussian spot shape. We aligned the major axis parallel to the x-axis of the photodiode. The output power at the end of the optical fiber is about 6.7 mW, measured with an optical power meter (PM20A, Thorlabs, USA). When the spot is focussed onto a gold coated cantilever (PPP-NCH-AuD, Nanosensors, Switzerland) the ratio of optical power above and below the cantilever is 10.2. The noise performance of three different PIN photodiodes was evaluated and it was found that the best SNR is produced by the S4349 (Hamamatsu, Japan). This photodiode is a four-quadrant Si PIN photodetector with 3 $\times$ 3 mm^2 active area, a dark current of 0.01 nA (@ $V_R = 5$ V), and a terminal capacitance (C_{PD}) of 50 pF (@ $V_R = 0$ V). The photodiode is driven without reverse voltage to reduce the dark current noise. The cut-off frequency without reverse voltage is large enough to use typical 300 kHz cantilevers for imaging.

Care was taken to keep the preamplifier board (green part in Fig. 3) in close proximity to the photodiode (white). It was not possible to mount the photodiode directly on the preamplifier board without modifying the original xy translation stage for the photodiode. The SLD beam can be moved by a xy-stage (XYPG-25, MISUMI Europa GmbH,Germany) with a nominal precision of 3 μm. The xy manoeuvring arrangement of the scanhead itself as well as that for the photodiode are original Bruker components.

We next turn to the description of the modified amplifier electronics. In Fig. 4, a simplified circuit diagram of the readout electronics is shown.

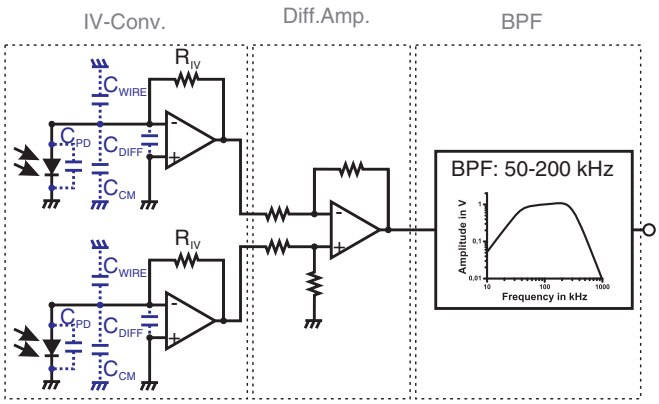

FIG. 4. (Color online) Simplified circuit diagram of the readout electronics, consisting of three parts, IV-converter, differential amplifier, and bandpass filter.

The photo current originating from each quadrant of the photodiode is amplified by an IV-converter consisting of an operational amplifier (OPA827, TI, USA) and a feedback resistor R_{IV}. The –3 dB bandwidth of the IV-converter (B_{IV}) is given by[14]

$$B_{IV} = \sqrt{\frac{GBP}{2\pi R_{IV} C_S}}, \tag{3}$$

where GBP is the gain bandwidth product (22 MHz for OPA827) of the operational amplifier and C_S is the source capacitance connected to the inverting input of the OPA. The used OPA has a comparatively small GBP but a good noise performance and the resulting bandwidth of the preamplifier is approximately 1 MHz, large enough to use typical 300 kHz cantilevers for imaging.

The differential amplifier is realized using a different OPA (LT1468, Linear Technology Corporation, Canada).

After the differential amplification, the signal is bandpass filtered. At a first glance, this additional filter might be useless, since the PLL circuit is very frequency-selective and should, therefore, act as very sharp bandpass. However, the used amplitude controller uses the root-mean-square value of the input signal to excite the cantilever, resulting in large additional noise inside the oscillator when using unfiltered input signals. By filtering the input signal with a bandpass filter, this additional noise can be reduced.

Figure 5 shows the frequency response of the preamplifier circuit and the total frequency response of the readout electronics. These frequency responses were measured with an intensity-modulated laser diode connected to a lock-in amplifier (Bruker, Nanoscope V controller). The frequency response of the laser diode is assumed to be constant in the measurement range.

The bandwidth of the bandpass filter was calculated to be 50–200 kHz and the measured bandwidth is $\approx$ 40–280 kHz as can be seen from Fig. 5. This range is sufficient for using different types of cantilevers in air and liquid environment.

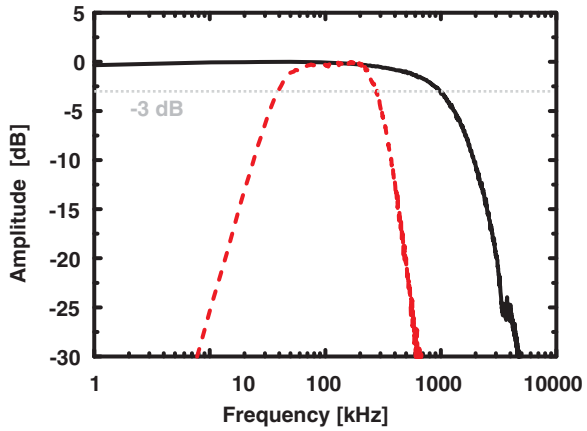

FIG. 5. (Color online) Frequency response of the preamplifier (black, solid) and the total readout electronics (red, dashed), measured with an intensity-modulated laser diode.

B. Open liquid cell

Ideal acoustic cantilever excitation requires the driving piezoelectric element to be placed directly below the cantilever base.[15] In many liquid cells including the original Bruker liquid cell, however, this is not realized in order to prevent damage to the driving piezo by, e.g., aggressive liquids. In order to directly excite the cantilever, we designed a new open liquid cell where the piezoelectric element is placed directly below the cantilever base. This design is very similar to the one presented in Ref. 16.

The new liquid cell (Fig. 6) is made of stainless steel, which makes it robust and easy to clean. The driving piezo and the cantilever base are surrounded by stainless steel (see Fig. 6(a)). To insulate the wires and the driving piezo from conductive aqueous solutions, a special rubber-like glue (EPO-TEK 310M, Epoxy Technology, Inc., USA) is filled in the space around the cantilever base. In this cell, the liquid is confined between the cover glass slide (L4343-6, Plano, Germany) and the sample surface. The cover glass is clamped and fixed with two screws (Fig. 6(b)). As the cover glasses are in direct contact with the sample solution, we decided to choose cheap glasses that can be changed easily. As a consequence, the used cover glasses are not anti-reflex coated. This reduces the laser power applied to the photodiode, thus the SNR is slightly reduced.

The liquid can be inserted between the cover glass and the sample surface with a syringe and a small needle.

This cell is very useful when different types of samples have to be investigated in a short time. When the sample system is changed the cantilever holder and all parts that come into contact with the sample system can be cleaned easily. The only disadvantage is the limitation of the scanning time to approximately one hour after all the liquid is evaporated. The evaporation process can be decelerated by increasing the humidity inside the isolation chamber.

C. Sample holder

We designed a sample holder for brittle crystals like calcite and calcium fluoride. The entire sample holder (Fig. 7)

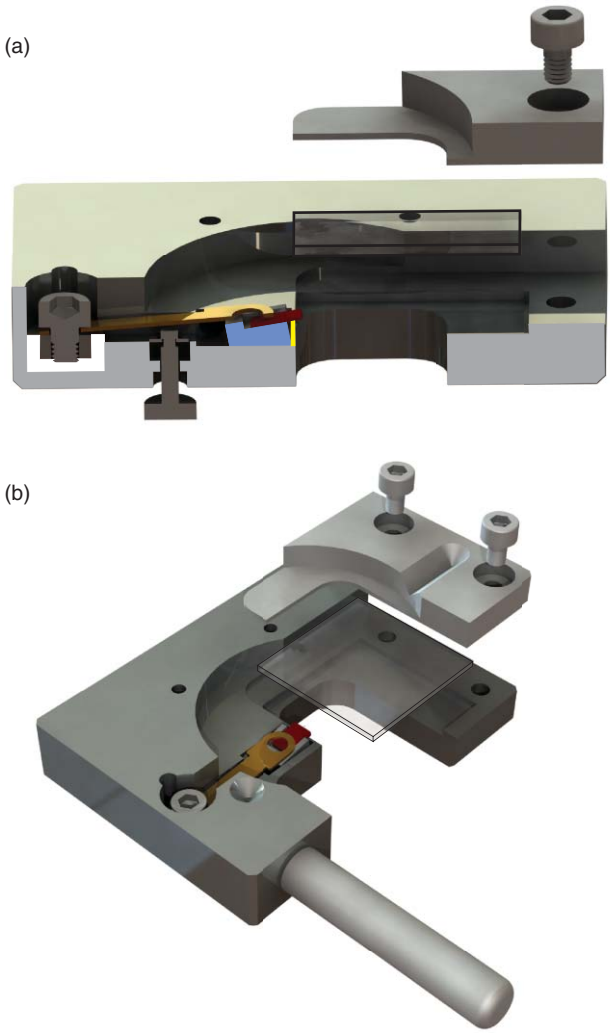

FIG. 6. (Color online) Model of home-built open liquid cell with cantilever holder.

measures 15 mm in diameter and is made of polyether ether ketone (PEEK). It is designed for crystals (shown as yellow part in Fig. 7) with dimension of 2×4 mm^2 and at least 3 mm in hight. At the top and bottom side of the main part, grooves are inserted, in which the cover plates can be pressed to seal the entire holder and make it waterproof. It should be noted that no glue is needed to seal the holder. This is of importance when working in liquids to ensure that the crystal surface is not polluted by dissolved components of the glue.

The crystals are clamped by a L-shaped piece of PEEK and a headless screw similar to the design presented in Ref. 17. This setup ensures that the crystal is orientated perfectly perpendicular to the cover plates. The crystal cleavage planes should be parallel to the 2×4 mm^2 side.

With this design it is very easy to cleave the crystals and to produce atomically flat surfaces. To cleave the crystal, the tip of a sharp scalpel is scratched over the side plane of the crystal along the edge of the cover plate until the breaking point is reached and the crystal is cleaved. Cleavage is induced by introducing a highly localized stress field acting at one point and breaking the crystal along a well defined lattice plane. Applying this procedure, it is straightforward to

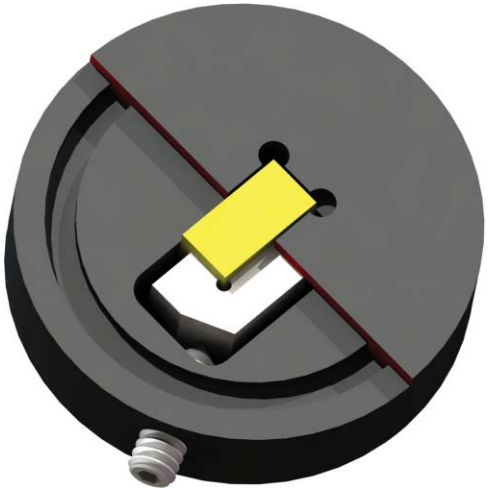

FIG. 7. (Color online) Model of home-built sample holder.

reproducibly generate surfaces with a small number of steps of a low height and very large atomically flat areas.[17]

D. Isolation chamber

The entire AFM is enclosed by a rigid isolation chamber as shown in Fig. 8. The whole enclosure consists of two parts. The main, inner chamber measures 50 × 50 × 50 cm^3 and is made of 2 cm thick aluminum sheets. The robust design has the advantage of effectively reducing acoustic noise. Moreover, when the chamber is grounded, it acts as a Faraday cage, effectively reducing the influence of external electrical fields. AC-magnetic fields (50 Hz), measured with a coil connected to a spectrum analyzer, are damped by a factor of four. In order to keep the temperature inside the chamber constant the entire compartment can be heated by resistors to 30–50 °C. The current through the resistors is controlled by a feedback circuit. The inner chamber is large enough to store samples inside, ensuring that the temperature of the samples, the AFM and the chamber are in equilibrium. This reduces thermal drift during the experiment.

Since the AFM base contains many active electronic parts, the base is located below the inner chamber. This makes temperature stabilization easier.

The outer chamber is an additional enclosure to shield the inner chamber from temperature variations in the lab.

A very important point is that this isolation chamber allows to monitor the cantilever and the sample with an on-top, highly magnifying camera (Bruker standard, also shown in Fig. 8), sensitive enough to control the laser alignment. Especially when operating in non-contact mode, a very save and gentle approach is required, typically ensured by a very slow software-controlled approach. The camera allows to manually approach the cantilever very close to the sample surface, greatly reducing the software-controlled approach distance.

V. PERFORMANCE OF THE DESCRIBED SYSTEM

In order to test the performance of the modified AFM, we measured the amplitude deflection noise density of the optimized system. Figure 9 shows the measured amplitude deflection noise densities d^z_{tot} for two typical cantilevers in air and liquid environment. The developed OBD sensor has a deflection noise density in the range of 5–15 fm/$\sqrt{\mathrm{Hz}}$ in air and liquid. As this value is below 20 fm/$\sqrt{\mathrm{Hz}}$, we can assume the frequency noise to be limited by the thermal noise (comp. Fig. (1)).

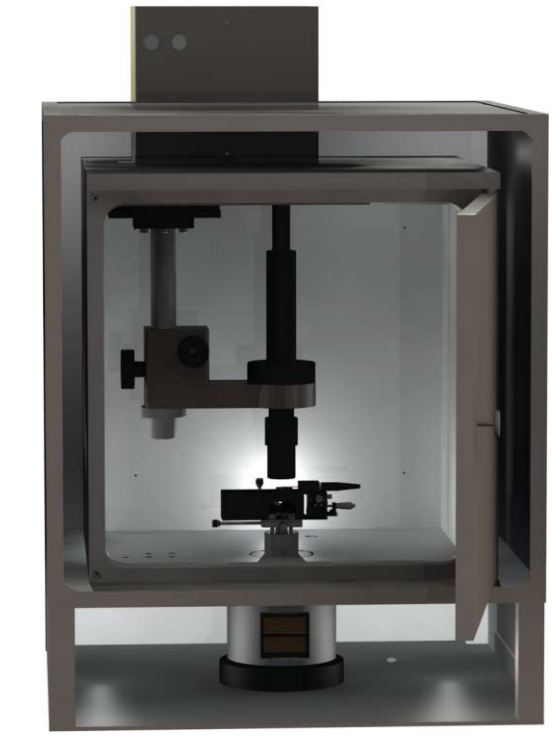

FIG. 8. (Color online) Model of home-built isolation chamber.

The optimized scanhead was integrated into a commercial Bruker MultiMode V system. Thermal stability and acoustic isolation are maintained by the developed isolation

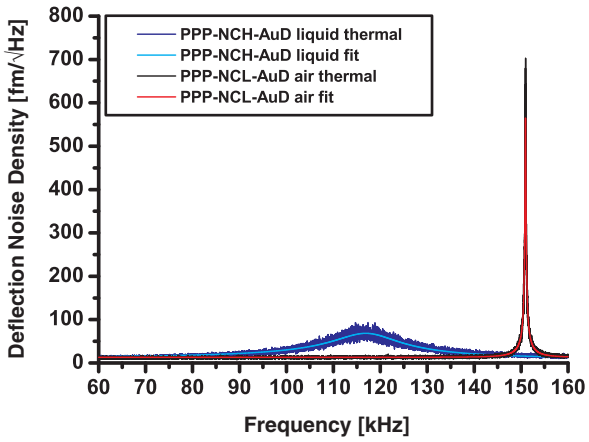

FIG. 9. (Color online) Measured deflection noise densities (as amplitude noise density) for two typical cantilevers. The amplitude sensitivity is de termined by fitting the thermal deflection noise density plus the constant deflection sensor noise density to the data. A fit for a NCL-AuD cantilever in air ($Q = 723$, $f_0 = 151$ kHz, sens = 4.4 nm/V, $k = 40$ N/m (assumed), $d^z_{\mathrm{el}} = 13$ fm/$\sqrt{\mathrm{Hz}}$), as well as a fit for a PPP-NCH-AuD cantilever in pure water ($Q = 8$, $f_0 = 117$ kHz, sens = 3.4 nm/V, $k = 40$ N/m (assumed), $d^z_{\mathrm{el}} = 10$ fm/$\sqrt{\mathrm{Hz}}$) are shown.

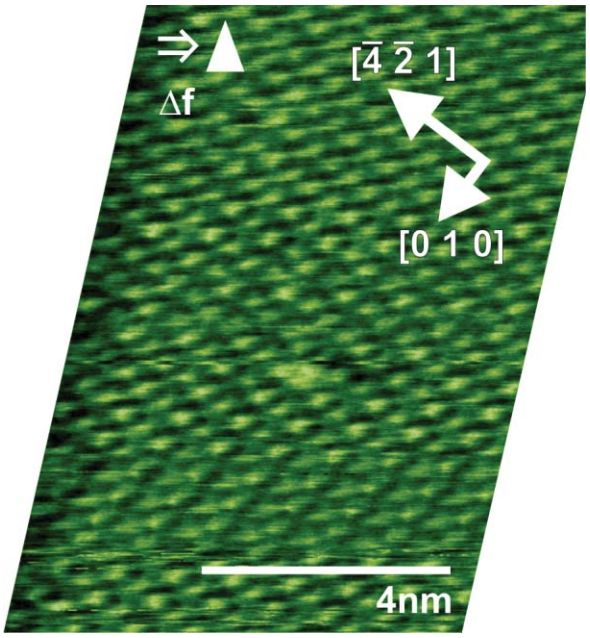

FIG. 10. (Color online) Drift-corrected, high-resolution image of the calcite ($10\bar{1}4$) cleavage plane.

chamber. Improved piezoelectric excitation is achieved by the developed fluid cell with integrated cantilever holder. We use Si cantilevers (PPP-NCH-AuD, Nanosensors, Switzerland), driven in the constant-amplitude mode. The oscillation amplitude was set to around 1 nm_{peak}. The scan speed was 10 nm/s and the frequency shift setpoint was set to +200 Hz. The thermal drift was compensated after imaging using SPIP (Image Metrology A/S, Denmark). Figure 10 shows an FM AFM image of calcite ($10\bar{1}4$) (see also Ref. 7) taken in a saturated calcite solution using the developed system. The tip-sample distance feedback was operated in the quasi-constant height mode (very slow feedback). The bandwidth and the lock range of the easyPLL was set to 1300 Hz and 1465 Hz, respectively.

As can be seen in Fig. 10, the atomic structure of calcite ($10\bar{1}4$) is clearly resolve in the image. Moreover, an atomic-scale defect is clearly visible, indicating the high-resolution capability of the developed system under liquid conditions.

ACKNOWLEDGMENTS

This work has been supported by the German Research Foundation (DFG) through KU1980/1-2 and GRA695. We gratefully acknowledge financial support by BASF SE.

The authors appreciate the contribution of J. Bystrzinski (precision engineering, University of Mainz), U. Klink and H. Heine (precision engineering, University of Osnabrück) and W. Schniederberend, D. Rathmann (electrical engineering, University of Osnabrück).

We are further grateful to H. Adam and S. Klassen for fruitful discussions and help throughout the modification process.

Last we would like to thank Bruker Nano Surfaces Division for fast and reliable support.

[1] T. Fukuma, M. Kimura, K. Kobayashi, K. Matsushige, and H. Yamada, Rev. Sci. Instrum. **76**, 053704 (2005).
[2] T. Fukuma and S. P. Jarvis, Rev. Sci. Instrum. **77**, 043701 (2006).
[3] B. W. Hoogenboom, P. L. T. M. Frederix, J. L. Yang, S. Martin, Y. Pellmont, M. Steinacher, S. Zaech, E. Langenbach, H. J. Heimbeck, A. Engel, and H. J. Hug, Appl. Phys. Lett. **86**, 074101 (2005).
[4] T. Fukuma, Rev. Sci. Instrum. **80**, 023707 (2009).
[5] S. Torbrügge, J. Lübbe, L. Tröger, M. Cranney, T. Eguchi, Y. Hasegawa, and M. Reichling, Rev. Sci. Instrum. **79**, 083701 (2008).
[6] T. Fukuma, K. Kobayashi, K. Matsushige, and H. Yamada, Appl. Phys. Lett. **87**, 034101 (2005).
[7] S. Rode, N. Oyabu, K. Kobayashi, H. Yamada, and A. Kühnle, Langmuir **25**, 2850 (2009).
[8] H. Yamada, K. Kobayashi, T. Fukuma, Y. Hirata, T. Kajita, and K. Matsushige, Appl. Phys. Express **2**, 095007 (2009).
[9] T. Fukuma, Jpn. J. Appl. Phys. **48**, 08JA01 (2009).
[10] K. Kimura, S. Ido, N. Oyabu, K. Kobayashi, Y. Hirata, T. Imai, and H. Yamada, J. Chem. Phys. **132**, 194705 (2010).
[11] T. Fukuma, Sci. Technol. Adv. Mater. **11**, 033003 (2010).
[12] K. Kobayashi, H. Yamada, and K. Matsushige, Rev. Sci. Instrum. **80**, 043708 (2009).
[13] F. J. Giessibl, Phys. Rev. B: Condens. Matter **56**, 16010 (1997).
[14] OPA827 data sheet.
[15] R. Motamedi and P. M. Wood-Adams, Sensors **8**, 5927 (2008).
[16] A. Maali, C. Hurth, T. Cohen-Bouhacina, G. Couturier, and J. P. Aime, Appl. Phys. Lett. **88**, 163504 (2006).
[17] L. Tröger, J. Schütte, F. Ostendorf, A. Kühnle, and M. Reichling, Rev. Sci. Instrum. **80**, 063703 (2009).